Full Text View

Volume 31, Issue 10 (October 2001)

Journal of Physical Oceanography
Article: pp. 2958–2970 | Abstract | PDF (1.14M)

Coastal-Trapped Waves and Tides at Near-Inertial Frequencies

Andrew C. Dale

College of Oceanic and Atmospheric Sciences, Oregon State University, Corvallis, Oregon

John M. Huthnance

Proudman Oceanographic Laboratory, Bidston Observatory, Merseyside, United Kingdom

Toby J. Sherwin

Centre for Applied Oceanography, Marine Science Laboratories, Anglesey, United Kingdom

(Manuscript received September 18, 2000, in final form March 6, 2001)

DOI: 10.1175/1520-0485(2001)031<2958:CTWATA>2.0.CO;2

ABSTRACT

The nature of the transition in coastal-trapped wave behavior from trapped, subinertial modes to imperfectly trapped, superinertial waves (not modes), is investigated. When formulated purely in terms of pressure, the coastal-trapped wave eigenvalue problem admits a spurious inertial mode that distorts numerical calculations at nearby frequencies. By solving a pair of coupled equations, involving the component of velocity normal to the coastline as well as pressure, this spurious mode is removed. The transition through the inertial frequency is examined analytically by considering the effect on trapped inertial modes of a small frequency increment. It is shown that, to first order in this increment, modes remain trapped. At higher frequencies, the modal approach breaks down and a primitive equation model is used to represent the, now fully three-dimensional, situation. The scattering of energy from an oscillating barotropic alongshore flow by a topographic feature is considered. At superinertial frequencies, internal energy is scattered in all directions, although preferentially alongshore in the direction of coastal-trapped wave propagation. There is not a sudden change in behavior at the inertial frequency. As frequency becomes increasingly superinertial there is a gradual increase in the three-dimensionality of the response and a decrease in the proportion of energy represented by the trapped component. The work highlights the potential for spurs and canyons to generate alongslope-propagating internal tides.

1. Introduction

The behavior of coastal-trapped waves near the inertial frequency is poorly understood, yet important in view of the energy concentrations at such frequencies. In linear theory, low frequency (subinertial) energy at ocean margins is channeled along topography and/or the coastline as coastal-trapped waves of various

types. At superinertial frequencies, however, linear theory admits free gravity waves and coastal-trapped waves cease to be perfectly trapped (Dale and Sherwin 1996, henceforth DS). This study investigates the nature of the transition from sub- to superinertial frequencies and discusses the changes in behavior that can be expected. One major motivation is to gain a greater understanding of the potential for alongshore transport of internal tidal energy within this frequency range. The M_2 tidal frequency (period 12.42 h) lies within 10% of the inertial frequency at all latitudes greater than 61.5°.

Coastal-trapped wave modes are generally calculated by solving a second-order equation describing perturbations in pressure in a vertical section normal to the coastline and topography. Unfortunately, close to the inertial frequency this approach becomes inaccurate because the pressure formulation admits a spurious (physically meaningless) inertial mode (Brink 1982). This spurious mode arises because boundary conditions involving the velocity component normal to the coast must be expressed in terms of pressure, but the relation between this component and pressure is singular at the inertial frequency. When modes are calculated numerically close to the inertial frequency, the spurious mode interacts with the physical modes of the system, causing dispersion curves to distort around the inertial frequency (DS).

An additional complication is a change in the nature of the governing differential equation from elliptic (subinertial) to hyperbolic (superinertial). Modal solutions to the superinertial coastal-trapped wave problem can never be entirely satisfactory due to difficulties in setting a realistic offshore boundary condition. Although modal shapes may appear acceptable close to the topography, they always contain components that either become large far offshore or require onshore phase and energy propagation from the ocean (DS). In addition, if the bed has points of critical slope at which the bed slope matches that of internal-wave characteristics, solutions may contain discontinuities that lie along characteristics. The difficulties with the modal approach are symptomatic of the increasing three-dimensionality of the problem, in the sense that the alongshore and cross-shore dependency are no longer separable when reasonable physical constraints (trapping conditions) are imposed. The modal approach becomes increasingly inappropriate as frequencies rise above the inertial frequency.

This paper begins by describing a method by which modes can be calculated accurately at near-inertial frequencies. The second-order pressure equation is replaced by a pair of equations involving pressure and the component of velocity normal to the coastline, enabling the boundary conditions to be set in a manner that remains valid at the inertial frequency. Similar techniques have been used in equatorial-wave calculations (e.g., Proehl 1991). The nature and implications of the transition from sub- to superinertial frequencies are then investigated analytically by considering slightly superinertial frequencies. At frequencies a finite interval above the inertial frequency, the breakdown of the modal approach necessitates solution of a fuller (and, in particular, three-dimensional) set of equations. To this end, the Bryan–Cox primitive equation model is used, first to make comparisons with the linear modal solutions, then to investigate the form of coastal-trapped waves generated by local forcing representing the interaction between an oscillating current and topography.

2. The coastal-trapped wave eigenvalue problem

Consider coastal topography of depth $h(x)$ that is uniform in the alongshore (y) direction (Fig. 1). Buoyancy frequency $N(z)$ is horizontally uniform. A motionless background state is perturbed by velocity components u, $\mathfrak{v}$, and w, pressure p, and density ρ. All these perturbations are expressed as functions of x and z in the form

$$u(x, y, z, t) = \mathrm{Re}\{u(x, z)\exp[i(ky - \sigma t)]\},$$

where $u(x, z)$ and wavenumber k may be complex but frequency σ is real. Thus, a nonzero imaginary component of k implies alongshore growth or decay. The linear, Boussinesq equations of motion are nondimensionalized with respect to scales L, U, f, H, ρ, N_0, HU/L, and ρfUL for horizontal position, velocity, frequency, depth, density, buoyancy frequency, vertical velocity, and pressure, respectively:

$$i\sigma u + \upsilon = \frac{\partial p}{\partial x} \qquad (1)$$

$$i\sigma \upsilon - u = ikp \qquad (2)$$

$$-\rho = \frac{\partial p}{\partial z} \qquad (3)$$

$$\frac{\partial u}{\partial x} + ik\upsilon + \frac{\partial w}{\partial z} = 0 \qquad (4)$$

$$i\sigma\rho + SN^2 w = 0, \qquad (5)$$

where u, $\mathfrak{v}$, w, ρ, p, σ, and k are now nondimensional, without change of notation. Two dimensionless parameters remain, $S \equiv N_0^2 H^2/f^2L^2$ and $D^2 \equiv f^2L^2/gH$ (which appears in the free-surface condition, below). Here L and H are taken to be the offshore and vertical scales of the topography, with $H = \lim_{x\to\infty} h(x)$. The hydrostatic approximation has been

made in (3), effectively assuming that $\sigma^2 \ll N^2$.

p formulation:

A second-order equation for p is obtained by expressing the velocity perturbations in terms of p:

$$u = \frac{i}{1 - \sigma^2}\left(\sigma\frac{\partial p}{\partial x} - kp\right), \tag{6}$$

$$v = \frac{1}{1 - \sigma^2}\left(\frac{\partial p}{\partial x} - k\sigma p\right), \quad \text{and} \tag{7}$$

$$w = \left(\frac{i\sigma}{SN^2}\right)\frac{\partial p}{\partial z}; \tag{8}$$

then substituting into the continuity equation (4)

$$\frac{1 - \sigma^2}{S}\frac{\partial}{\partial z}\left(\frac{\partial p/\partial z}{N^2}\right) + \frac{\partial^2 p}{\partial x^2} - k^2 p = 0. \tag{9}$$

Boundary conditions are a free surface

$$i\sigma D^2 p + w = 0 \Rightarrow D^2 SN^2 p + \frac{\partial p}{\partial z} = 0 \quad (z = 0), \tag{10}$$

no flow through the bed

$$w + u\frac{dh}{dx} = 0 \Rightarrow \left(\frac{1 - \sigma^2}{SN^2}\right)\frac{\partial p}{\partial z} + \frac{dh}{dx}\left(\frac{\partial p}{\partial x} - \frac{k}{\sigma}p\right) = 0 \quad (z = -h(x)), \tag{11}$$

and a coastal wall

$$u = 0 \Rightarrow \sigma\frac{\partial p}{\partial x} - kp = 0 \qquad (x = 0). \tag{12}$$

The open ocean is assumed to be flat bottomed, so perturbations in this region can be decomposed into a linear combination of vertical structure modes with horizontal structure arranged to match the alongshore wavenumber k (DS). The vertical structure mode eigenvalue problem for pressure perturbations $p'(z)$ is

$$\frac{1 - \sigma^2}{S}\frac{d}{dz}\left(\frac{dp'/dz}{N^2}\right) = \kappa^2 p' \tag{13}$$

with boundary conditions $D^2SN^2p' + dp'/dz = 0$ at the surface ($z = 0$) and $dp'/dz = 0$ on the bed ($z = -1$). The nth vertical mode $p'_n(z)$ has eigenvalue κ_n, related to component wavenumbers k and l_n in the y and x directions respectively through

$$\kappa^2_n = k^2 + l^2_n. \tag{14}$$

Thus, the decomposition at the offshore boundary is written

$$p(x, z) = \sum_{n=1}^{\infty} a_n p'_n(z) \exp(l_n x), \tag{15}$$

where the a_n are coefficients to be determined. The sign of each l_n is chosen to ensure offshore decay, although, when k is complex, this choice may not be consistent with a second trapping condition, that energy flux can only be outward through the boundary (DS).

The relation (6) between u and p is singular at the inertial frequency ($\sigma = 1$), leading to problems with the boundary conditions (11) and (12) when the problem is expressed purely in terms of pressure. A spurious inertial "mode,"

$$p(x, z) = A(z) \exp(kx), \quad (16)$$

where $A(z)$ is an arbitrary function that satisfies the surface boundary condition, is a solution to the pressure-formulated problem for any k, although the underlying physical problem is not necessarily satisfied. A more careful treatment of the inertial frequency is required (next section).

u, p formulation

In order to avoid the spurious mode, (9) is replaced by two independent equations in u and p: (6) and

$$\frac{\partial u}{\partial x} + \frac{ik^2}{\sigma} p + \frac{k}{\sigma} u + \frac{i\sigma}{S} \frac{\partial}{\partial z} \left(\frac{\partial p / \partial z}{N^2} \right) = 0, \quad (17)$$

which is implied by (2), (4), and (8). Boundary conditions are also expressed in terms of u and/or p. The surface condition (10) is unchanged and no flow through the bed is written as

$$\frac{i\sigma}{SN^2} \frac{\partial p}{\partial z} + u \frac{dh}{dx} = 0 \qquad (z = -h(x)). \quad (18)$$

The coastal condition is

$$u = 0 \qquad (x = 0), \quad (19)$$

and the flat-bottomed open ocean is again treated by decomposition into vertical structure modes, now of the coupled u,p system.

3. Expansion about the inertial frequency

At the inertial frequency, (1) and (2) together imply that $\partial p / \partial x = kp$, so inertial modes can be written in the form $p(x, z) = p_0(z) \exp(kx)$. It will be seen that inertial modes occur at discrete values of k, in contrast to the spurious mode (16) that occurs at all k. Expanding to a slightly superinertial frequency $\sigma = 1 + \epsilon$ (where $\epsilon \ll 1$), solutions are written

$$\Phi(x, z) = \{\Phi_0(z) + \epsilon \Phi_1(x, z)\} \exp(kx), \quad (20)$$

where $k = k_0 + \epsilon k_1$ with Φ representing p, u, v, w, or ρ. Equations (1)–(5) become

$$i(1 + \epsilon)(p_0 + \epsilon p_1) + SN^2(w_0 + \epsilon w_1) = 0. \qquad (25)$$

On the bed

$$(w_0 + \epsilon w_1) + \frac{dh}{dx}(u_0 + \epsilon u_1) = 0 \qquad (z = -h(x)), \qquad (26)$$

and at the free surface

$$iD^2(1 + \epsilon)(p_0 + \epsilon p_1) + (w_0 + \epsilon w_1) = 0 \qquad (z = 0). \qquad (27)$$

Order ϵ^0: Inertial solutions

From the order ϵ^0 terms of (21)–(25), u_0 and w_0 can be expressed in terms of p_0 as

$$u_0 = -\frac{i}{2}\left[\frac{1}{k_0 S}\frac{d}{dz}\left(\frac{dp_0/dz}{N^2}\right) + k_0 p_0\right] \quad \text{and} \qquad (28)$$

$$w_0 = \frac{i dp_0/dz}{SN^2}. \qquad (29)$$

The bed condition (26) then yields a differential equation in $p_0(z)$,

$$\frac{d}{dz}\left(\frac{E dp_0/dz}{N^2}\right) + k_0^2 S E p_0 = 0, \qquad (30)$$

where $E = \exp(2k_0 X)$ and $X(z)$ is defined by $z = -h(X)$ with $X = 0$ at $z = 0$. Boundary conditions on $p_0(z)$ are

$$\frac{dp_0}{dz} + D^2 SN^2 p_0 = 0 \qquad (z = 0) \qquad (31)$$

at the surface and

$$\frac{dp_0}{dz} = 0 \qquad (z = -1) \qquad (32)$$

far offshore where the bed is flat ($w = 0$).

Together, (30), (31), and (32) constitute a one-dimensional Sturm–Liouville system for $p_0(z)$ with eigenvalues of S (Huthnance 1978). Thus, for fixed wavenumber k_0, inertial modes exist at discrete values of the stratification parameter S. The spurious nature of the inertial mode of the pressure-formulated problem (9)–(12) and (15) is now apparent since $p(x, z) = \exp(kx)$ was a solution for any combination of k and S. Note that, if inertial modes are sought with fixed S and eigenvalues of k_0, the problem is no longer in Sturm–Liouville form. There will always be an essentially barotropic Kelvin-like mode (assuming the surface is free), but there may be no baroclinic modes when S is small, since coastal-trapped wave dispersion curves do not necessarily reach the inertial frequency.

Order ϵ^1: Near-inertial solutions

The order ϵ^1 terms of (21)–(25) are

$$\rho_1 + \frac{\partial p_1}{\partial z} = 0, \tag{35}$$

$$k_0 u_1 + \frac{\partial u_1}{\partial x} + ik_0 v_1 + \frac{\partial w_1}{\partial z} = -k_1 u_0 - ik_1 v_0, \quad \text{and} \tag{36}$$

$$i\rho_1 + SN^2 w_1 = -i\rho_0. \tag{37}$$

The bed condition is

$$w_1 + \frac{dh}{dx} u_1 = 0 \qquad (z = -h(x)) \tag{38}$$

and the free surface

$$iD^2 a(p_0 + p_1) - w_1 = 0 \qquad (z = 0). \tag{39}$$

From (33), (34), and the ϵ^0 terms of (24)

$$\frac{\partial p_1}{\partial x} = \frac{1}{k_0 S} \frac{d}{dz}\left(\frac{dp_0/dz}{N^2}\right) \equiv P(z), \tag{40}$$

defining $P(z)$, which can be calculated from the inertial solution. Integrating in x,

$$p_1(x, z) = xP(z) + Q(z), \tag{41}$$

where $Q(z)$ remains to be determined. Proceeding by expressing u_1 and w_1 in terms of the inertial solution, then using the bed condition (38), it is straightforward to obtain

$$w_1 = \frac{i}{SN^2}\left(\frac{dp_0}{dz} + x\frac{dP}{dz} + \frac{dQ}{dz}\right) \tag{42}$$

and more involved to obtain

$$\frac{\partial}{\partial x}(u_1 E) = -ik_0 E\left[k_1\left(p_0 - \frac{P}{k_0}\right) + xk_0 P + \frac{x}{k_0 S}\frac{d}{dz}\left(\frac{dP/dz}{N^2}\right) + \frac{3P}{2} - \frac{k_0 p_0}{2} + k_0 Q + \frac{1}{k_0 S}\frac{d}{dz}\left(\frac{dQ/dz}{N^2}\right)\right], \tag{43}$$

using (30), (34), (36), and (40). Integration yields u_1, with the constant of integration (a function of z) set to zero to ensure $u = 0$ far offshore. Substitution into (38), and further manipulation involving (30) and (40), results in an equation for Q,

$$= k_1 E\left(\frac{p_0}{k_0} - p_0\right) - xk_0 EP - \frac{E}{k_0 S}\frac{d}{dz}\left(\frac{dP/dz}{N^2}\right)$$

$$+ \frac{E}{2k_0^2 S}\frac{d}{dz}\left(\frac{dP/dz}{N^2}\right) + \frac{3}{2}k_0 E p_0, \qquad (44)$$

in which the first-order deviation of wavenumber k_1 remains to be determined. Boundary conditions on Q are

$$\frac{dQ}{dz} + D^2 S N^2 Q = 0 \qquad (z = 0) \qquad (45)$$

at the free surface and

$$\frac{dQ}{dz} = 0 \qquad (z = -1) \qquad (46)$$

at the maximum depth. Wavenumber k_1, which effectively gives the gradient of the dispersion curve through the inertial frequency, is found by projecting (44) onto the inertial mode $p_0(z)$ of the Sturm–Liouville system by multiplying by p_0 and integrating in z. The left-hand side of (44) becomes

$$\left[\frac{E}{k_0 S N^2}\left(\frac{dQ}{dz}p_0 - Q\frac{dp_0}{dz}\right)\right]_{-1}^{0}$$

$$+ \int_{-1}^{0} Q\left[\frac{1}{k_0 S}\frac{d}{dz}\left(\frac{E dp_0/dz}{N^2}\right) + k_0 E p_0\right] dz, \qquad (47)$$

which is zero in view of (30) and the boundary conditions on Q and p_0. The full equation (44), after several integrations by parts, yields

$$2k_1\left[\int_{-1}^{0} E\left(p_0^2 + \frac{p_0(dX/dz)(dp_0/dz)}{k_0 S N^2}\right) dz\right]$$

$$= \frac{3}{2}\int_{-1}^{0} E k_0 p_0^2 \, dz + \frac{1}{2k_0}\int_{-1}^{0} EP^2 \, dz$$

$$+ \frac{1}{2k_0^2 S}\left[\frac{p_0(dP/dz) - (dp_0/dz)P}{N^2}\right]_{-1}^{0}, \qquad (48)$$

using (30), (40), $X = 0$ at $z = 0$ and $E \longrightarrow 0$ as $z \longrightarrow -1$.

Note, in particular, that k_1 must be real since all other terms in this expression are real. Thus, to first order above the inertial frequency, wavenumber remains real (as it is at subinertial frequencies). The problems that arise in setting the open boundary condition for complex k must only become apparent at higher order.

4. Comparative linear solutions

Comparisons are now made between numerical solutions of the two-dimensional p formulated eigenvalue problem [(9)–(12) and (15)], the equivalent u, p formulated problem [(6), (17), (10), and (19)] and the one-dimensional inertial eigenvalue problem [(30)–(32)]. Dimensional variables will be used from this point onward, and a rigid lid assumed ($D = 0$), removing the barotropic Kelvin-like mode.

Topography and stratification are prescribed analytically, loosely based on the Iberian shelf around 40°N. Bottom depth is

$$h(x) = \begin{cases} h_c + (h_{\text{match}} - h_c)x/x_{\text{match}}, & x \le x_{\text{match}} \\ h_s + \left\langle \frac{1}{2}\left\{1 - \cos\left[\frac{\pi}{W}(x - x_s)\right]\right\}\right\rangle^{3/4} (h_o - h_s), & x_s + W > x > x_{\text{match}} \\ h_o, & x \ge x_s + W, \end{cases} \quad (49)$$

(Click the equation graphic to enlarge/reduce size)

where h_c = 50 m, h_s = 100 m, and h_o = 3100 m are the depths at a coastal wall (x = 0), at the shelf edge ($x = x_s$ = 12 km), and in the ocean ($x > x_s + W$), respectively; W = 31 km is the width of the slope. The shelf slants linearly to a depth h_{match} at $x = x_{\text{match}}$, values chosen such that the depth and gradient of the shelf and slope match, and in practice very close to h_s and x_s. Note that a flat shelf has been avoided since it would imply a singularity $|X_z| \to \infty$ in (30). The flat ocean floor leads to a similar singularity at $z = -h_o$, although the inertial eigenvalue problem is still solvable with this singular endpoint. The buoyancy frequency is surface intensified, decreasing exponentially with a vertical scale of z_0 = 500 m:

$$N^2 = 2.7 \times 10^{-5} \exp(z/z_0)\ \text{s}^{-2}. \quad (50)$$

Computations are made on a (vertically stretched) Σ grid with 20 equally spaced vertical levels and 50 horizontal levels (Δx = 1000 m). The u, p formulation has u and p levels staggered in x. The coastal wall is placed at a u level, and the upper and lower levels lie on the surface and bed respectively. Solutions are found by a resonance-searching approach (DS), in which the hyperbolic or elliptic system is inverted subject to forcing of some wavenumber and frequency (following Lindzen and Kuo 1969). The response is large close to a dispersion curve, so, by scanning through values of frequency and wavenumber, dispersion curves can be mapped out in (k, σ) space. When the scanned resonance field is displayed as a grayscale image (Figs. 2 and 4), dispersion curves appear as lines of enhanced resonance (dark).

In the p formulated case, the effect of the spurious inertial mode on dispersion curves is clear (Fig. 2), with strong distortion of the lowest mode within the range $\sigma/f \in [0.9, 1.1]$ such that the subinertial and superinertial segments of its dispersion curve bend to avoid crossing the inertial frequency. This distortion is a purely numerical effect since the p and u, p formulations are entirely equivalent at any noninertial frequency. Distortion reduces when grid resolution is improved (Fig. 3) and is greatest for higher, less well resolved modes. The u, p formulated problem has no apparent inertial distortion (Fig. 4, with dispersion curves closely matching those of Fig. 2 away from the inertial frequency).

The change in the nature of the problem from elliptic to hyperbolic is evident through noise in the superinertial resonance fields (Figs. 2 and 4) and modal shapes (Fig. 5). This noise is due to inability to resolve the discontinuities and/or strong gradients that arise in cases with critical or near-critical bed slope. Dale and Sherwin also encountered noisy resonance fields, although, in their case of uniform buoyancy frequency, resolution was less critical and the noise less severe. Investigation of the effect of varying computational resolution on subinertial (σ/f = 0.9) eigenvalues (Table 1) suggests that the calculated values are close to convergence. The same is true of superinertial (σ/f = 1.1) eigenvalues (Table 2), although they converge less predictably. In determining these (complex) superinertial eigenvalues, the offshore boundary condition has been set as described by DS.

The one-dimensional inertial eigenvalue problem, defined by (30)–(32), can be solved efficiently at high resolution. This provides a check on the accuracy of the modes of the two-dimensional p and u, p formulated problems. We again consider the topography (49) with stratification (50) and seek eigenvalues of k. Solution is carried out on a grid with vertical intervals of unform spacing Δz. Resolution tests (Table 3) suggest that, when 1000 levels are used, the eigenvalues have almost converged to the accuracy quoted (four significant figures). Modal pressure fields take the form $p(x, z) = p_0(z) \exp(kx)$, with $p_0(z)$ for the first three modes shown in Fig. 6. Agreement with the dispersion curves of the coupled u, p system is excellent (Fig. 4), with a discrepancy of less than 1% in wavenumber. Equivalent nonhydrostatic calculations (Table 3) demonstrate that, for this problem, the hydrostatic approximation was justified.

For a given inertial solution, the first-order perturbation k_1 to wavenumber $k = k_0 + \epsilon k_1$ at slightly superinertial frequencies $\sigma/f = 1 + \epsilon$ can be evaluated directly using (48). The first three inertial modes have $k_1 = -0.532 \times 10^{-4}$, -1.205×10^{-4}, and -2.063×10^{-4} m^{-1}, respectively (calculated from the corresponding 10 000 level solutions), with the implied gradient of the dispersion curves agreeing closely with the resonance scans of the coupled u, p system (Fig. 4).

5. Response of a primitive equation model

Since a superinertial coastal-trapped wave has inherent three-dimensionality and cannot be perfectly described as a mode, a primitive equation model (the Bryan–Cox model: Cox 1984; Semtner 1985) will be used to investigate the differences between slightly superinertial and slightly subinertial waves. The Bryan–Cox model is nonlinear, Boussinesq, hydrostatic, has a rigid lid, and uses a z grid in which coordinate levels are horizontal, so there are fewer vertical grid levels in shallow water. Although viscosity and diffusion are set to zero, the model has some inherent numerical viscosity and mixing.

Simulations are made in dimensional coordinates, with an identical physical setting to the linear results of the previous section. Grid spacings are Δx = 2 km, variable Δy (see next section), and 20 vertical levels of uneven spacing, providing improved resolution toward the surface (8 × 25 m, 5 × 100 m, 4 × 200 m, 2 × 500 m, and 1 × 600 m). Alongshore boundaries are cyclic, the onshore boundary is walled, and the offshore boundary is open (Stevens 1990). It is not immediately obvious that such a model will well represent coastal-trapped waves such as those calculated in the previous section, so this question is addressed first.

a. Dispersion relations from a primitive equation model

Consider a shelf edge topography of finite alongshore extent, but with periodic alongshore boundary conditions (Fig. 7). Such a model domain has an effective alongshore wavenumber $k = \pm 2\pi/\lambda$, where λ is its alongshore extent. From an initial rest state the model is subjected to periodic forcing of frequency σ and integrated for five forcing cycles. By varying λ and σ, the amplitude of the model response can be mapped out in dispersion space in a manner analogous to the approach used for the linear eigenvalue problem. The alongshore grid spacing $\Delta y = \lambda/20$ scales with λ, so the alongshore length scale of interest is always equally resolved. The forcing need not have any physical significance since the aim is merely to determine the tendency of the model to respond to various frequencies and length scales in the forcing. In practice, a perturbation to the barotropic streamfunction is applied with sinusoidal form alongshore, decreasing linearly from its oceanic amplitude to zero at the coast. The forcing amplitude is kept as small as is numerically acceptable to ensure that the model response is, to a good approximation, linear. A growth rate for the background model kinetic energy is determined by taking the time series of total model kinetic energy, determining the best fit $\partial(\mathrm{KE})/\partial t$ by linear regression, then normalizing this by the maximum kinetic energy of the imposed perturbation, which varies with λ.

When topography and stratification are equivalent to those used in the modal calculations, resonances of the model agree remarkably well with modal dispersion curves (Figs. 4, 8, and 9). The form of the response at resonance peaks also matches the calculated linear modes well (Fig. 5). Note, in particular, that the resonance fields show no discernible change in model behavior at the inertial frequency. The close agreement gives confidence that the Bryan–Cox model is representing well the low modes of the linear, modal calculations, providing justification for the wave generation experiments that follow.

b. Wave generation by an oscillating alongshore flow interacting with topography

The model domain of the previous section is extended to 750 km alongshore, and a spur is added by displacing the topography offshore by a Gaussian function of width 20 km (alongshore) and amplitude 20 km (offshore). Forcing is provided by an oscillating alongshore flow applied as a periodic perturbation to the barotropic streamfunction. This perturbation is a function of offshore distance only and is not modified by the spur, so the interaction between the spur and forcing flow is not accurately represented. In effect, the spur acts as a localized source of internal energy, and interest here is in the nature of the response away from the generation region. Peak velocities of the forcing current are small (0.01 m s^{-1}, with total excursions of order 100 m) ensuring that the response is largely linear and is dominated by the forcing frequency. Nonlinearity of the model does, however, mean that other frequencies are also present.

Three forcing frequencies are considered: slightly subinertial (σ/f = 0.9), slightly superinertial (σ/f = 1.1), and more strongly superinertial (σ/f = 1.5). The response in each case consists of a train of coastal-trapped waves at the forcing frequency and a radial scattering of nontrapped internal “ripples” from the spur (Fig. 10). Evanescent modes (e.g., Webster and Holland 1987), which could potentially spread energy in the direction opposite to trapped, wave propagation, need not be considered here because they occur only when trapped wave dispersion curves peak at a subinertial frequency. The magnitude of the anomalies associated with the trapped component are similar at each forcing frequency (Fig. 11, series A), with 0.05°C at 350 m corresponding to a vertical displacement of 5.5 m. In each case, the trapped component has a clear wavelength that matches linear predictions for a mode 1 coastal-trapped wave. This wavelength decreases with frequency as expected.

The relative importance of the nontrapped response increases with frequency. At σ/f = 1.5, time series (Fig. 11) of the temperature anomaly offshore of the spur (C) and alongshore in the direction opposite to coastal-trapped wave propagation (B) contain primarily the forcing frequency. Vertical displacements are an order of magnitude smaller than the trapped response. At the near-inertial forcing frequencies (σ/f = 0.9 and σ/f = 1.1) the nontrapped response is weaker since energy at these frequencies is unable to propagate freely (σ/f = 0.9) or propagates only slowly (σ/f = 1.1). In each case, frequency spectra of the temperature anomaly at B and C peak above the forcing frequency, representing nonlinear transfer of energy to higher frequency, more rapidly propagating modes.

6. Discussion and conclusions

A previous work (DS) discussed the differences between linear coastal-trapped waves at sub- and superinertial frequencies. However, there remained considerable questions regarding the behavior of coastal-trapped waves close to the inertial frequency and the nature and significance of the transition through the inertial frequency. Here, the aim has been to improve understanding of the near-inertial frequency range and gain insight into the sub-/superinertial distinction, including the question of whether wave trapping suddenly breaks down at the inertial frequency, or whether there is a gradual transition in wave behavior.

Pressure-formulated linear theory is inaccurate close to the inertial frequency due to a spurious inertial mode. The

approach of using a coupled *u*, *p* formulation is computationally more expensive than a *p*-only formulation, but has been successful in removing the spurious mode and consequent near-inertial distortion of the physical modes. Still, the *u*, *p* formulated problem is only of practical use in mode calculation at subinertial frequencies because the noise resulting from unresolved discontinuities/shear above the inertial frequency potentially dominates the calculations. This problem with shear is a failing of linear theory since, in reality, it would tend to be smoothed by friction and/or mixing. Perhaps more reliable superinertial calculations could be made by parameterizing this friction in some way, as, for instance, in linear internal tidal theory (e.g., Chuang 1980).

One-dimensional linear calculations at the inertial frequency both confirm the accuracy of the two-dimensional *u*, *p* calculations, and suggest that, to first order in a small frequency increment, modes remain perfectly trapped as they become superinertial. This is significant in that it suggests a smooth transition in wave behavior at the inertial frequency, rather than a catastrophic breakdown of the linear approach.

A further problem with linear theory is the increasing three-dimensionality of the problem, in the sense that a modal description (in which alongshore dependence is written as a, possibly complex, wavenumber) becomes increasingly inappropriate as frequency rises above the inertial frequency. To gain some intuition for the three-dimensional nature of the superinertial problem, the nonlinear, primitive equation Bryan–Cox model was used. When wave amplitudes were kept small to maintain near-linearity, it was found that the model supported coastal-trapped waves that agreed very closely in structure and wavenumber/frequency with corresponding linear calculations, despite the apparently crude resolution used. Of course, although the Bryan–Cox model can represent the full three-dimensionality of the problem, it is unable to resolve the strong shears of linear theory, so this failing is common to all the approaches used.

Generation experiments involved an oscillating, barotropic, alongshore current interacting with a spur protruding from the shelf edge. These experiments were highly idealized and intended to give an intuitive impression of the differing behavior of locally generated sub- and superinertial internal energy in the presence of a topographic “channel” of propagation (the shelf edge slope and coastline). A gradual change was found in the response to increasing frequency, with no clear distinction between sub- and superinertial frequencies. The balance between the trapped and nontrapped components of the generated internal wave field increasingly favored the more three-dimensional, nontrapped component as frequency increased, but there was no sudden transition in behavior. Of course, in reality, subinertial trapped waves lose energy both through friction and nonlinear transfer of energy to higher, nontrapped frequencies. Superinertial waves would be expected to lose energy more rapidly since energy at the wave frequency itself is imperfectly trapped and potentially scattered offshore by topographic irregularities.

It is still not clear to what extent near-inertial or superinertial energy is channeled alongshore or along topography in the ocean. The Bryan–Cox model runs give a graphic illustration of the potential for spurs and canyons to generate alongshore-propagating internal tides. It would obviously be interesting to model more realistic settings, with realistic topography and forcing. The extent to which offshore scattering of energy by alongshore variations in topography would lead to enhanced decay of such coastal-trapped waves could also be addressed. Whether the (here inadequately resolved) shears that occur at superinertial frequencies modify wave behavior significantly or lead to significant energy loss is an important and perhaps more difficult problem.

Acknowledgments

This work was largely funded as part of the OMEX (Ocean Margin Exchange) project, European Union Contract MAS2-CT93-0069.

REFERENCES

Brink K. H., 1982: A comparison of long coastal-trapped wave theory with observations off Peru. *J. Phys. Oceanogr*, **12**, 897–913. Find this article online

Chuang W.-S., 1980: Propagation and generation of internal tides on the continental margin. Ph.D. thesis, Johns Hopkins University, 114 pp.

Cox M. D., 1984: A primitive equation, three-dimensional model of the ocean. GFDL Ocean Group Tech. Rep. No. 1, 143 pp. [Available from Geophysical Fluid Dynamics Laboratory/NOAA, Princeton University, Princeton, NJ 08542.].

Dale A. C., and T. J. Sherwin, 1996: The extension of baroclinic coastal-trapped wave theory to superinertial frequencies. *J. Phys. Oceanogr*, **26**, 2305–2315. Find this article online

Huthnance J. M., 1978: On coastal trapped waves: Analysis and numerical calculation by inverse iteration. *J. Phys. Oceanogr*, **8**, 74–92. Find this article online

Lindzen R. S., and H.-L. Kuo, 1969: A reliable method for the numerical integration of a large class of ordinary and partial differential equations. *Mon. Wea. Rev*, **97**, 732–734. Find this article online

Proehl J. A., 1991: On the numerical dispersion relation of equatorial waves. *J. Geophys. Res*, **96**, 16929–16934. Find this article online

Semtner A. J., 1985: Finite difference formulation of a world ocean model. *Advanced Physical Oceanographic Numerical Modelling*, J. J. O'Brien, Ed., D. Reidel, 187–202.

Stevens D. P., 1990: On open boundary conditions for three dimensional primitive equation ocean circulation models. *Geophys. Fluid Dyn*, **51**, 103–133. Find this article online

Webster I., and D. Holland, 1987: A numerical method for solving the forced baroclinic coastal-trapped wave problem of general form. *J. Atmos. Oceanic Technol*, **4**, 220–226. Find this article online

Tables

TABLE 1. Resolution dependency of the modes of the *u*, *p* formulated eigenvalue problem. Eigenvalues are of k (m^{-1}) for fixed frequency $\sigma/f = 0.9$

Mode number	k (10 Σ levels, Δx = 2 km)	k (20 Σ levels, Δx = 1 km)	k (30 Σ levels, Δx = 0.5 km)
1	-0.425×10^{-4}	-0.429×10^{-4}	-0.430×10^{-4}
2	-0.971×10^{-4}	-0.950×10^{-4}	-0.945×10^{-4}
3	-1.896×10^{-4}	-1.678×10^{-4}	-1.628×10^{-4}

Click on thumbnail for full-sized image.

TABLE 2. Resolution dependency of the modes of the *u*, *p* formulated eigenvalue problem at frequency $\sigma/f = 1.1$

Resolution	k, mode 1
10 Σ levels, Δx = 2 km	$-0.543 \times 10^{-4} - 0.007 \times 10^{-4}i$
20 Σ levels, Δx = 1 km	$-0.548 \times 10^{-4} - 0.002 \times 10^{-4}i$
30 Σ levels, Δx = 0.5 km	$-0.546 \times 10^{-4} - 0.003 \times 10^{-4}i$

Click on thumbnail for full-sized image.

TABLE 3. Wavenumber k (m^{-1}) of modes of the one-dimensional inertial eigenvalue problem (30)–(32) for varying resolution. The first two columns are hydrostatic, the third is nonhydrostatic

Mode number	k (1000 levels)	k (10 000 levels)	k (10 000 levels, nonhydrostatic)
1	-0.490×10^{-4}	-0.489×10^{-4}	-0.490×10^{-4}
2	-1.104×10^{-4}	-1.104×10^{-4}	-1.105×10^{-4}
3	-1.883×10^{-4}	-1.884×10^{-4}	-1.887×10^{-4}

Click on thumbnail for full-sized image.

Figures

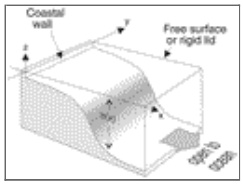

Click on thumbnail for full-sized image.

FIG. 1. Configuration of axes

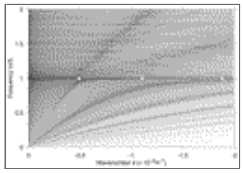

Click on thumbnail for full-sized image.

FIG. 2. Resonance scan for the two-dimensional problem formulated in terms of *p* only. Shading has a log scale, with dark corresponding to strong resonance. Topography is given by (49) and buoyancy frequency by (50); Δx = 1000 m, 20 vertical levels. White circles indicate solutions of the corresponding one-dimensional inertial eigenvalue problem

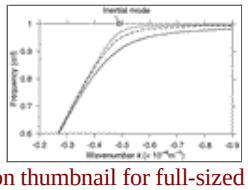

Click on thumbnail for full-sized image.

FIG. 3. Near-inertial distortion of the lowest subinertial-mode dispersion relation at three different computational resolutions: Δx = 2000 m, 10 vertical levels (solid line); Δx = 1000 m, 20 vertical levels (dashed line); and Δx = 500 m, 30 vertical levels (dotted line). A white circle indicates the mode of the corresponding one-dimensional inertial eigenvalue problem

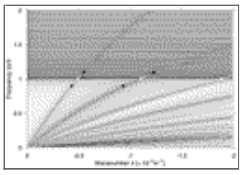

Click on thumbnail for full-sized image.

FIG. 4. Resonance scan for the two-dimensional problem formulated in terms of both u and p. Topography is given by (49) and buoyancy frequency by (50); Δx = 1000 m, 20 vertical levels. White circles indicate solutions of the corresponding one-dimensional inertial eigenvalue problem, with the gradient of the dispersion curves implied by calculated k_1 shown. Black circles indicate resonances of the Bryan–Cox model at σ/f = 0.9 and σ/f = 1.1

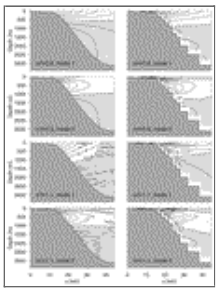

Click on thumbnail for full-sized image.

FIG. 5. Comparative modal shapes of the u, p formulated linear problem (left column, as the real part of the pressure perturbation p) and at corresponding resonances of the Bryan–Cox model (right column, as an alongshore velocity $\mathfrak{V}$). Shading represents sign, and the scaling is arbitrary. The first two modes are shown at subinertial and superinertial frequencies σ/f = 0.9 and σ/f = 1.1, respectively

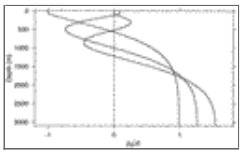

Click on thumbnail for full-sized image.

FIG. 6. Vertical pressure distribution $p_0(z)$ of the first three inertial modes. Topography is given by (49) and buoyancy frequency by (50). Wavenumbers $k = -0.489 \times 10^{-4}$, $k = -1.104 \times 10^{-4}$, and $k = -1.883 \times 10^{-4}$ m^{-1}

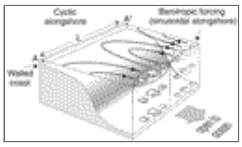

Click on thumbnail for full-sized image.

FIG. 7. A schematic representation of the method used to determine the response of the Bryan–Cox model to forcing at varying frequency σ and alongshore length scale λ. Alongshore boundaries are cyclic, so A and A′ are the same point

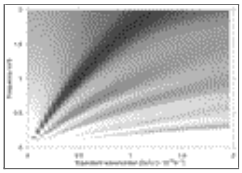

Click on thumbnail for full-sized image.

FIG. 8. Background kinetic energy growth rate of the Bryan–Cox model when subject to forcing of varying frequency σ and alongshore scale λ. Dark shading indicates strong resonance. The shading scale is not linear. The relative strength and wavenumber extent of resonances can be seen in Fig. 9

Click on thumbnail for full-sized image.

FIG. 9. Kinetic energy growth rate for the Bryan–Cox model when forced with frequency $\sigma/f = 0.9$ (solid) or $\sigma/f = 1.1$ (dashed) and varying effective wavenumber $2\pi/\lambda$

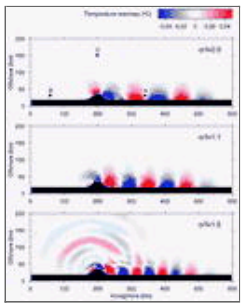

Click on thumbnail for full-sized image.

FIG. 10. Temperature anomaly at 350 m after three inertial periods of forcing by an alongshore flow oscillating at three different frequencies: slightly subinertial ($\sigma/f = 0.9$), slightly superinertial ($\sigma/f = 1.1$), and strongly superinertial ($\sigma/f = 1.5$). A temperature anomaly of 0.05°C corresponds to a vertical displacement of 5.5 m

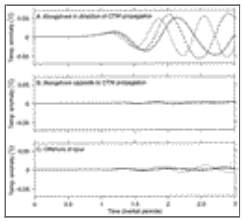

Click on thumbnail for full-sized image.

FIG. 11. Time series of temperature anomaly at 350-m depth for the three locations A, B, and C of Fig. 10 and three forcing frequencies $\sigma/f = 0.9$ (solid line), $\sigma/f = 1.1$ (dashed line), and $\sigma/f = 1.5$ (dotted line)

Corresponding author address: Dr. Andrew C. Dale, College of Oceanic and Atmospheric Sciences, Oregon State University, 104 Ocean Admin. Bldg., Corvallis, OR 97331-5503. E-mail: acd@oce.orst.edu

top